# Electronic structure, effective mass, and optical dispersion of 2-mercapto-5-methyl-1,3,4-thiadiazole: density functional theory calculations

Sikander Azam [a], A.H. Reshak [a,b,*]

[a] *New Technologies Research Centre, University of West Bohemia, Univerzitni 8, 306 14 Pilsen, Czech Republic*
[b] *Center of Excellence for Geopolymers and Green Technology, School of Material Engineering, University Malaysia Perlis, 01007 Kangar, Perlis, Malaysia*

A R T I C L E   I N F O

A B S T R A C T

Density functional theory was used to calculate the electronic band structure, effective mass, and optical dispersion of 2-mercapto-5-methyl-1,3,4-thiadiazole (MMTD). The all-electron, full-potential, linearized augmented plane wave method was used. The exchange correlation potential was treated using the local density approximation, generalized gradient approximation, and modified Becke Johnson approximation. The calculated band structure shows that MMTD has a direct energy bandgap. The partial density of states revealed strong hybridization between N p, C p, N s, and H s orbitals. The electronic charge density distribution confirmed partial ionic and strong covalent C–N, C–C, C–H, and N–N bonds. We also calculated the optical dielectric function and related optical properties (refractive index, extinction coefficient, absorption coefficient, and reflectivity).

© 2014 Elsevier Ltd. All rights reserved.

## 1. Introduction

Mercapto-functionalized thiadiazoles have been widely investigated for applications such as bioactive compounds, chelating agents, lubricant additives including corrosion inhibitors and anti-wear agents, polymer cross-linkers, and cathode components of battery schemes [1–3]. One of the most interesting properties of mercapto-substituted thiadiazoles is the existence of thiol and thione tautomers, since tautomerization effects on the reactivity of thiadiazoles have been observed for polymerization processes [2], substitution reactions at diverse moieties [1,4], and metal complexation [5]. The tautomeric equilibrium of mercapto thiadiazoles has been a controversial issue [6,7]. Most

authors have suggested that the thione form is the prevailing species according to vibrational spectroscopy evidence [6], but the existence of the thiol form has also been discussed [7]. However, no comprehensive structural study combining vibrational spectroscopy, X-ray investigations, and theoretical analyses has been reported so far.In a study of thermolysis behaviors, Hipler et al. investigated the tautomeric equilibria and structures of 2,5-dimercapto-1,3,4-thiadiazole and 2-mercapto-5-methyl-1,3,4-thiadiazole (MMTD, Fig. 1) using ab initio and density functional theory (DFT) computations [8]. They found that the thione-thiol and thione tautomer were the most stable [9]. Spectral data for MMTD indicate that the thione tautomer exists predominantly in DMSO solution and in the solid state [8]. The molecular structure of MMTD in the solid state has been investigated by single-crystal X-ray diffraction since some spectroscopic investigations indicated the presence of the thioamide tautomer, but the molecular arrangement and level of hydrogen bonding

---

* Corresponding author at: New Technologies Research Centre, University of West Bohemia, Univerzitni 8, 306 14 Pilsen, Czech Republic.
*E-mail address:* maalidph@yahoo.co.uk (A.H. Reshak).

were not known. Hipler et al. optimized and calculated the tautomer frequency using the B3LYP functional as applied in the Gaussian 03 bundle, which is a non-full potential procedure [8]. In general, the B3LYP functional disregards van der Waals interactions, which leads to inaccuracy.

Many theoretical approaches have been used to identify the bandgap of materials. For example, the optimized effective potential procedure and many-body perturbation theory give excellent bandgap values in comparison to experimental data [10–12], but this approach is computationally costly. Other possibilities include local density approximation (LDA)+U and generalized gradient approximation (GGA)+U [13], which can be applied only for correlated and localized 3d or 4f electrons in transition metal and rare-earth oxides. This is a very successful but



**Fig. 1.** Molecular and unit cell structure of 2-mercapto-5-methyl-1,3,4-thiadiazole.

very expensive method [9]. A good alternative that overcomes the above-mentioned problems is the modified Becke-Johnson (mBJ) exchange potential approximation [14]. This computationally inexpensive technique can accurately describe the electronic structure of semiconductors and insulators.

In the present study we investigated MMTD using the all-electron full-potential linear augmented plane wave method. Our calculated bond lengths and angles show good agreement with experimental values [9]. This is because the geometry of the solid structure is subject to intermolecular forces, such as van der Waals interactions and crystal packing forces. Therefore, the full-potential method is suitable and gives significant insight into the origin of the band structure and density of states (DOS). This confirms that it is very important to use a full-potential method.

## 2. Computational methodology

MMTD has an orthorhombic structure with space group Pbca. The unit cell and molecular structure are shown in Fig. 1. Self-consistent calculations were carried out using the full-potential linearized augmented plane wave (FP-LAPW) method as implemented in the WIEN2k code [15]. Exchange–correlation was solved based on the LDA [16], GGA of Perdew–Burke–Ernzerh [17], and the mBJ approximation. We used XRD crystallographic data taken from CCDC 195453 [8]. We optimized the atomic positions by minimizing the forces acting on the atoms. From the relaxed geometry, the electronic structure, electronic charge density, and optical properties can be determined. The optimized and experimental geometries are compared in Table 1 and reveal good agreement. We calculated the bond lengths and angles, which also show good agreement with experimental data (Tables 2 and 3). The agreement between calculated and experimental data confirms the accuracy of our method.

For the core and valence states, we applied the full relativistic calculation and its scalar approximation, respectively. Values of the muffin-tin sphere radius ($R_{MT}$) were chosen as 1.00 a.u. for N, 1.110 a.u. for C, 0.540 a.u.
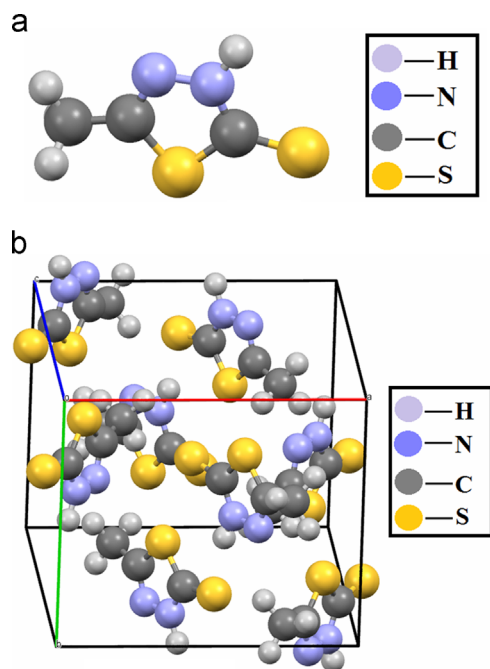
**Table 1**
Optimized (Opt) atomic positions in comparison to experimental (Exp) data (CCDC 195453) [9].

| Atom | Atomic positions | | | | | |
|------|------|------|------|------|------|------|
| | X | | Y | | Z | |
| | Exp | Opt | Exp | Opt | Exp | Opt |
| S1 | 0.61457(7) | 0.61345 | 0.23289(8) | 0.22864 | 0.59773(6) | 0.59747 |
| S2 | 0.46181(8) | 0.46138 | 0.12015(8) | 0.11627 | 0.80112(6) | 0.80290 |
| C2 | 0.5512(2) | 0.5503 | 0.0972(3) | 0.0913 | 0.6843(2) | 0.6850 |
| N3 | 0.5872(2) | 0.5876 | −0.0318(2) | 0.9601 | 0.64032(18) | 0.6411 |
| H3 | 0.5653 | 0.5632 | −0.1127 | 0.8567 | 0.6728 | 0.6750 |
| N4 | 0.6594(2) | 0.6609 | −0.0332(2) | 0.9594 | 0.54273(19) | 0.5426 |
| C5 | 0.6817(2) | 0.6825 | 0.0990(3) | 0.0946 | 0.5099(2) | 0.5095 |
| C51 | 0.7572(3) | 0.7574 | 0.1353(3) | 0.1337 | 0.4059(2) | 0.4059 |
| H51A | 0.8005 | 0.8075 | 0.0489 | 0.0353 | 0.3794 | 0.3743 |
| H51B | 0.8187 | 0.8271 | 0.2099 | 0.2210 | 0.4241 | 0.4258 |
| H51C | 0.7011 | 0.6937 | 0.1707 | 0.1765 | 0.3471 | 0.3381 |

**Table 2**
Bond lengths in comparison to experimental data (CCDC 195453) [9].

| Bond | Length (Å) | |
| --- | --- | --- |
| | Experimental | Optimized |
| S1–C2 | 1.730(3) | 1.7466 |
| S1–C5 | 1.743(3) | 1.7517 |
| S2–C2 | 1.670(2) | 1.6789 |
| C2–N3 | 1.337(3) | 1.3578 |
| N3–H3 | 0.860(2) | 1.0536 |
| N3–N4 | 1.369(3) | 1.3851 |
| N4–C5 | 1.285(3) | 1.3103 |
| C5–C51 | 1.488(3) | 1.4878 |
| C51–H51A | 0.960(3) | 1.1022 |
| C51–H51B | 0.961(3) | 1.1049 |
| C51–H51C | 0.961(3) | 1.1075 |

**Table 3**
Bond angles in comparison to experimental data (CCDC 195453) [9].

| Bond | Bond angle (°) | |
| --- | --- | --- |
| | Experimental | Optimized |
| C2–S1–C5 | 90.0(1) | 90.12 |
| S1–C2–S2 | 127.2(1) | 126.51 |
| S1–C2–N3 | 107.1(2) | 107.40 |
| S2–C2–N3 | 125.7(2) | 126.09 |
| C2–N3–H3 | 120.5(2) | 125.09 |
| C2–N3–N4 | 119.0(2) | 118.59 |
| H3–N3–N4 | 120.5(2) | 116.31 |
| N3–N4–C5 | 109.9(2) | 109.67 |
| S1–C5–N4 | 114.0(2) | 114.23 |
| S1–C5–C51 | 122.7(2) | 121.97 |
| N4–C5–C51 | 123.3(2) | 123.80 |
| C5–C51–H51A | 109.5(2) | 109.26 |
| C5–C51–H51B | 109.5(2) | 110.48 |
| C5–C51–H51C | 109.5(2) | 110.41 |
| H51A–C51–H51B | 109.5(3) | 109.91 |
| H51A–C51–H51C | 109.5(3) | 109.50 |
| H51B–C51–H51C | 109.4(3) | 107.25 |



**Fig. 2.** Calculated electronic band structure of 2-mercapto-5-methyl-1,3,4-thiadiazole.

for H, and 1.490 a.u. for S. A mesh of 1500 **k**-points in the irreducible wedge of the first Brillouin zone (BZ) was used. A plane-wave cutoff of $R_{MT}^{*}k_{max} = 8.0$ and harmonic expansion up to $l_{max} = 10$ were assumed throughout the computations.

## 3. Results and discussion

### 3.1. Band structure

Most of the physical properties of solids are directly or indirectly related to the electronic band structure. Thus, knowledge of the bandgap is important for efficient use of materials in optoelectronic, magneto-optic, and electromagnetic devices [18]. Fig. 2 shows the calculated band structure along the high-symmetry directions (R→Γ→X→M→Γ) for MMTD using LDA, GGA, and mBJ approaches. The band structures calculated using the three approximations are generally similar. The valence band maximum (VBM) and conduction band minimum (CBM) are located at the center of the BZ, resulting in a direct
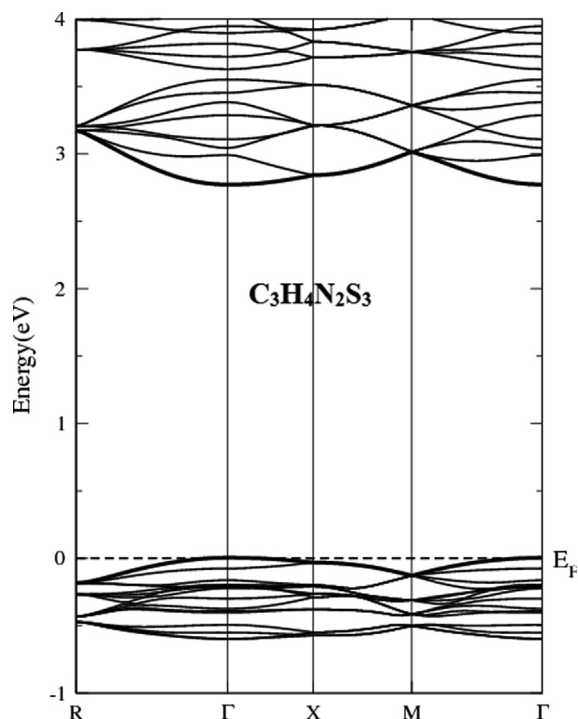
bandgap of approximately 3.75 eV according to the mBJ approach, which is much better than the LDA and GGA results [19–22]. Compounds with a direct bandgap are optically active and are suitable for photonic and optoelectronic devices. Unfortunately, there are no experimental or theoretical data on the MMTD bandgap for comparison to our computed results.

### 3.2. Density of states

To identify distinct states of the electronic structure and the nature of fundamental energy bandgap of MMTD, the total and partial DOS, and the contribution of individual states are illustrated in Fig. 3. For the lowest energy band of MMTD, between −11.22 and −6.0 eV, there is strong hybridization between N p and H s states. The second structure between −6.0 eV and the Fermi level mainly comprises S s, N p, S p, and C p states, with a small contribution from H s and C s states. In the lower VB there is strong hybridization between S s and S p states. In MMTD the p states of N and C atoms make the major contribution to the VB. Furthermore, p-like states of C, N, and S atoms contribute more to the lower VB, with minor contributions from S s and C p states, while p states of N and S contribute more to the upper VB. The lower CB is a complex mixture of p states of S, C, and N atoms.

Analysis of the partial DOS reveals hybridization between N p, C p, N s, and H s orbitals. Thus, we can conclude that MMTD also has some covalent features in spite of its major ionic character.
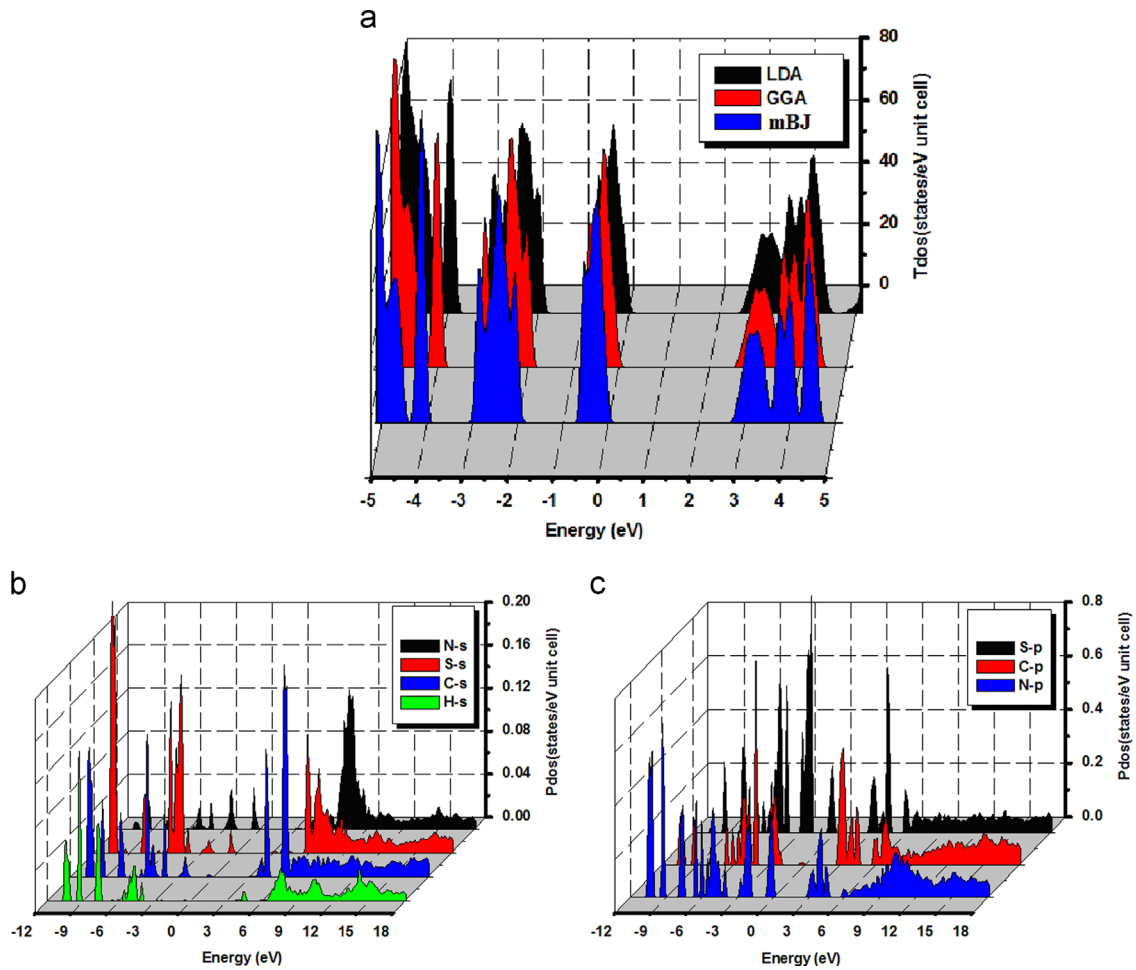
**Fig. 3.** Calculated total and partial densities of states (states/eV unit cell) for 2-mercapto-5-methyl-1,3,4-thiadiazole.

### 3.3. Electronic charge density

We analyzed the electronic charge density to obtain an insight into the electronic structure. Fig. 4 shows the electronic charge density contour for the (1 1 0) crystallographic plane. The contour plot shows partial ionic and strong covalent C–N, C–C, C–H, and N–N bonds as a result of the Pauling electronegativity difference between C (2.550), H (2.200), S (2.580), and N (3.04) atoms. The contour plots reveal that the majority of the electronic charge for C, H, and S atoms is transferred to N atoms. This can be easily seen from the color charge density scale, where blue (+1.0000) corresponds to the maximum charge-accumulating site. The charge density along C–N, C–C, C–H, and N–N bonds is pronounced because of the strong hybridization of covalent C–N, C–C, and C–H bonds. We should highlight that the charge density distribution is basically spherical around all atoms. We also plotted the electron charge density distribution in the (1 0 −1) crystallographic plane to investigate anisotropy between the two planes in the crystal. The contour plots for the (1 1 0) and (1 0 −1) planes demonstrate that the MMTD crystal possesses considerable anisotropy, which favors enhanced optical susceptibility. It is clear from Fig. 4 that the charge

density contour around the S atom is more circular in the (1 0 −1) plane than in the (1 1 0) plane. The distance between S and H atom in (1 1 0) plane is shorter than in the (1 0 −1) plane.

We calculated the bond lengths and angles, and these show good agreement with experimental data [9].

### 3.4. Effective mass

The effective charge carrier mass $m^*$ was evaluated by fitting the $E$–$\mathbf{k}$ diagram using a paraboloid around the VBM or CBM. We calculated the effective electron mass ($m_e^*$) from the curvature of the CBM (band no. 155) for MMTD. The diagonal elements of the effective mass tensor for electrons in the conduction band are calculated in the $\Gamma \rightarrow \Gamma$ direction in $\mathbf{k}$ space using the following well-known relation:

$$\frac{1}{m_e^*} = \frac{1}{\hbar^2} \frac{\partial^2 E(k)}{\partial k^2}. \tag{1}$$

The effective electron mass is determined by fitting the CBM to a parabolic function described by Eq. (3) in the first BZ using the EVGGA approach. The effective electron mass ratio ($m_e^*/m_e$) calculated for MMTD around $\Gamma$ is 0.0577.
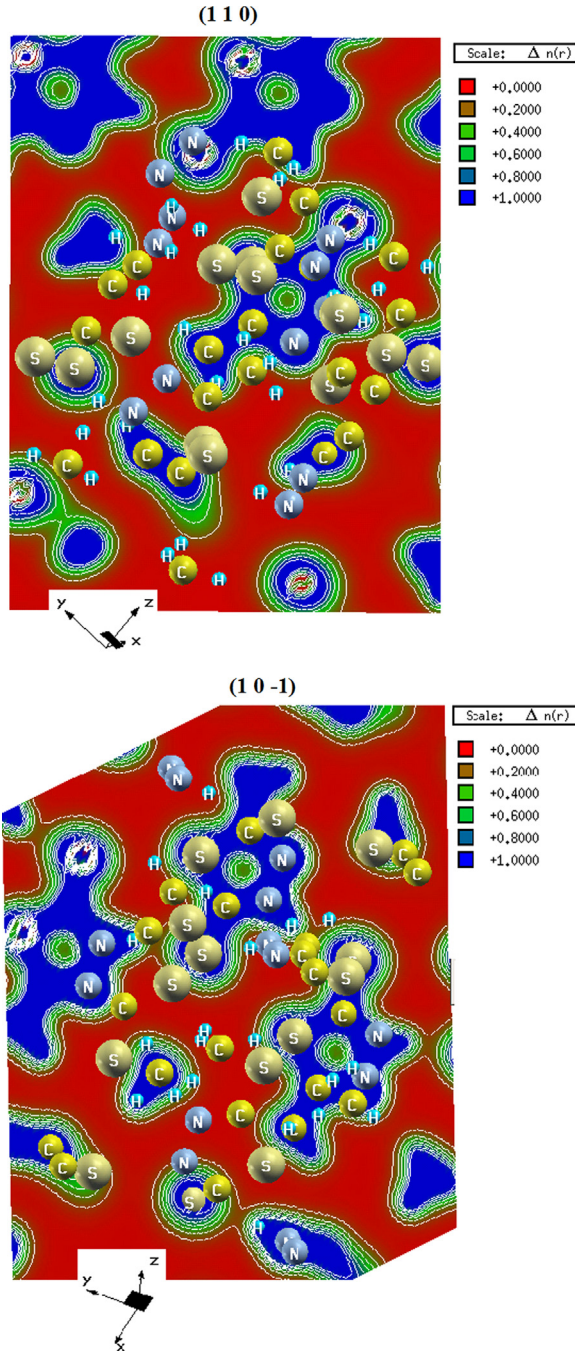
**(1 1 0)**



**(1 0 -1)**



**Fig. 4.** Electronic charge density contour for 2-mercapto-5-methyl-1,3, 4-thiadiazole.

Using the same procedure, we also calculated the effective mass of heavy holes and light holes from the curvature of the VBM and the next valence band. These values were 0.1126 and 0.0757 for heavy and light holes, respectively.

### 3.5. Dispersion of optical parameters

Optical spectroscopy analysis is a powerful tool for determining the overall band behavior of a solid [23–26].

The linear responses of optical parameters were calculated using equations described in the literature [27,28]. In the solid state, electron–phonon interactions play a principal role [29]. The imaginary part of the optical dielectric tensor is obtained directly from the calculated electronic structure by means of the joint DOS and transition matrix elements [30]:

$$\varepsilon_2^{ij}(\omega) = \frac{8\pi^2\hbar^2 e^2}{m^2 V} \sum_k \sum_{cv} (f_c - f_v) \frac{p_{cv}^i(k)p_{vc}^j(k)}{E_{vc}^2} \delta[E_c(k) - E_v(k) - \hbar\omega],$$

(2)

where $m$ is the electron mass, $e$ is the electron charge, $\hbar$ is Plank's constant, and $f_c$ and $f_v$ are the Fermi distributions of the CB and VB, respectively. The term $p_{cv}^i(k)$ denotes the momentum transition in energy for matrix elements from level $c$ of the CB to level $v$ of the VB at a certain **k**-point in the BZ, and $V$ is the unit cell volume. Eq. (2) gives the relation between solid macroscopic optical constants and the band structure, transition matrix elements, and DOS. Therefore, we can calculate and analyze macroscopic optical parameters such as the refractive index, absorption coefficient, and reflectivity using the Kramers–Kronig dispersive relation.

The dielectric function, as a bridge between the microphysical process of interband electron transitions and the electronic structure, can reflect the energy band structure of a solid and other types of spectral information. Using the electronic structure, the frequency-dependent optical dielectric functions of MMTD were calculated. Fig. 5 shows the imaginary part $\varepsilon_2(\omega)$ and real part $\varepsilon_1(\omega)$ of the optical dielectric function calculated for three different light polarizations. The frequency-dependent dielectric functions $\varepsilon_2^{xx}(\omega)$, $\varepsilon_2^{yy}(\omega)$, and $\varepsilon_2^{zz}(\omega)$ show considerable anisotropy. The peak magnitude is considerably greater for $\varepsilon_2^{yy}(\omega)$ and $\varepsilon_2^{zz}(\omega)$ than for $\varepsilon_2^{xx}(\omega)$.

The threshold (critical) point of $\varepsilon_2(\omega)$ occurs at $\sim$2.3 eV, which is related to a direct transition from the VBM to the CBM at the $\Gamma$ point. The $\varepsilon_2^{xx}(\omega)$, $\varepsilon_2^{yy}(\omega)$, and $\varepsilon_2^{zz}(\omega)$ spectra exhibit six strong transition peaks in the energy range between 0.0 and 14.0 eV. To identify these peaks, we need to consider the magnitude of the optical matrix elements. The observed peaks should correspond to transitions that have large optical matrix elements. The data presented confirm substantial anisotropy of the calculated band structure.

From the partial DOS for C, H, N and S atoms, we conclude that the interband transitions can be attributed to excitation of the N p state to the C s state at $<$3.0 eV. The second transition occurs from an S p orbital to a H s or N s orbital.

The real part of the dielectric function, $\varepsilon_1(\omega)$, is evaluated from the imaginary part $\varepsilon_2(\omega)$ using the Kramers–Kronig relation. The real part is illustrated in Fig. 5b. It is evident that at low energy $\varepsilon_1(\omega)$ increases with energy, with a first peak at 3.0 eV for $\varepsilon_1^{xx}(\omega)$ and $\varepsilon_1^{zz}(\omega)$ and at 3.5 eV for $\varepsilon_1^{yy}(\omega)$. The peak height decreases with increasing photon energy. Values calculated for the real part at the static limit are $\varepsilon_1^{xx}(0) = 1.4$, $\varepsilon_1^{yy}(0) = 1.51$, and $\varepsilon_1^{zz}(0) = 1.53$y.

Fig. 6a–d shows the calculated absorption spectrum, refractive index, reflectivity, and energy loss spectrum
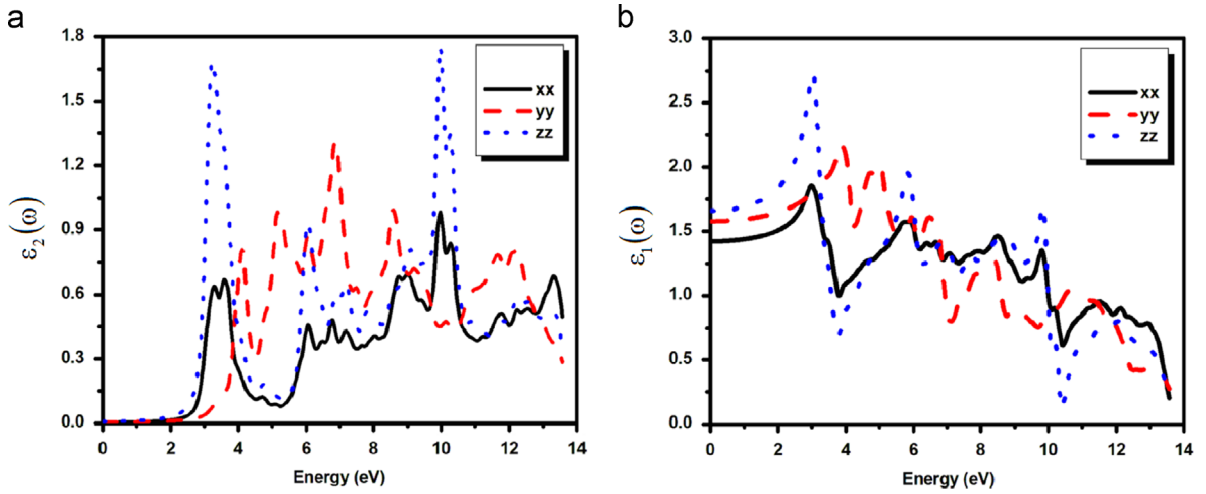
**Fig. 5.** Calculated imaginary $\varepsilon_2(\omega)$ and real $\varepsilon_1(\omega)$ parts of the dielectric tensor for 2-mercapto-5-methyl-1,3,4-thiadiazole.
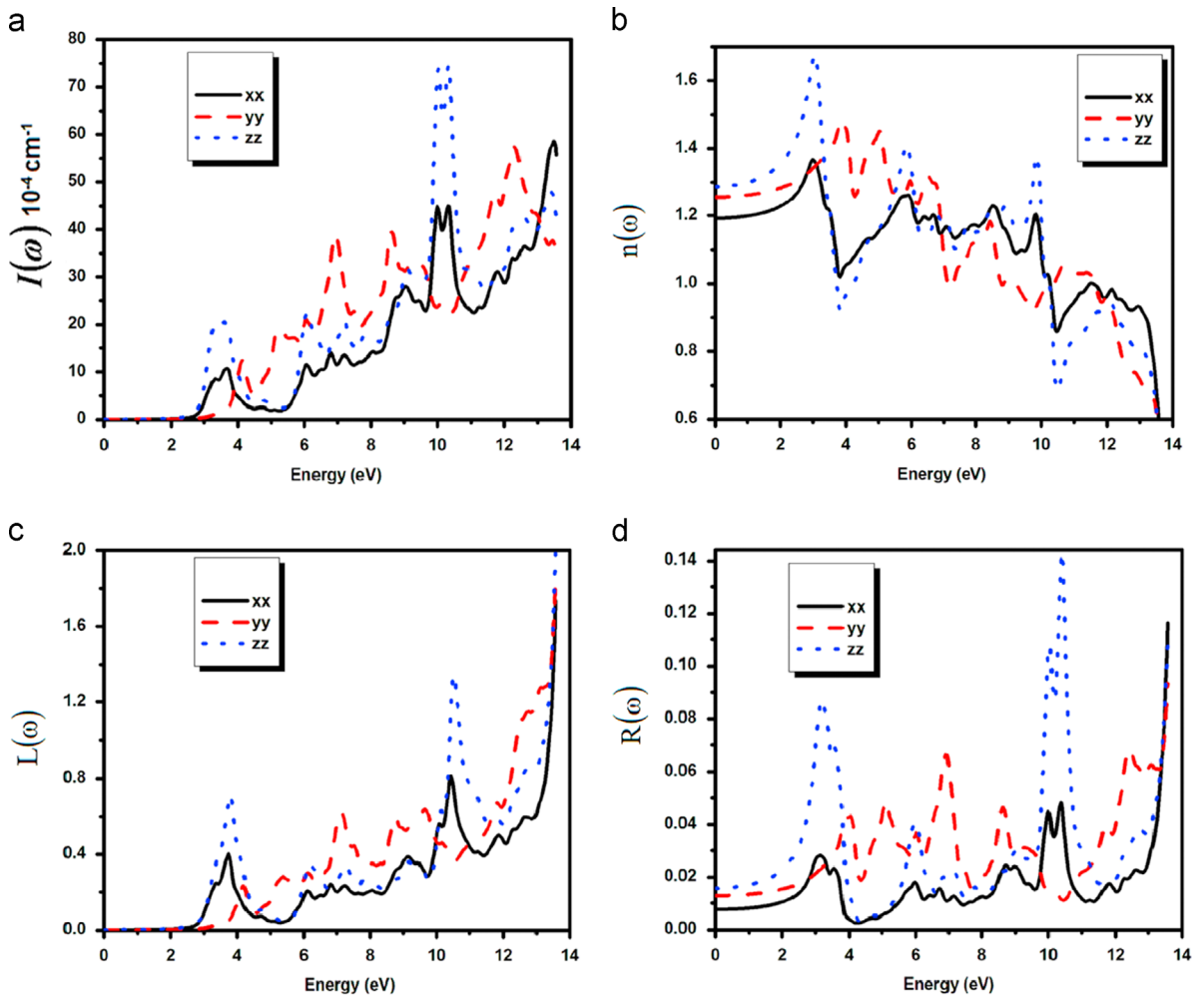


**Fig. 6.** Calculated absorption spectrum $I(\omega)$, refractive index $n(\omega)$, energy-loss spectrum $L(\omega)$ and the reflectivity $R(\omega)$ for 2-mercapto-5-methyl-1,3,4-thiadiazole.

for MMTD. The absorption edge begins at approximately 2.9 eV (Fig. 6a), corresponding to the $\Gamma_V$–$\Gamma_C$ energy gap. The absorption edge can be attributed to a transition from the N p state at the VBM to the C p state at the CBM. The first peak in the absorption spectrum is at 3.5 eV, with other peaks located at 4.2, 5.5, and 10.5 eV.

The refractive index (Fig.6b) of the crystal is closely related to the electronic polarizability of ions and the local field within the crystal. The average value of $n(0)$ is 1.236. In Fig. 6b a spectral maximum can be observed between 2.0 and 5.5 eV. At intermediate energies many small peaks appear and then the curves vanish at higher energies. The reason for these vanishing curves at higher energy is that beyond a certain energy the material is no longer transparent and it absorbs high-energy photons and the refractive index falls below unity. Static values of the refractive index were found to be $n^{xx}(0) = 1.18$, $n^{yy}(0) = 1.25$, and $n^{zz}(0) = 1.28$. The refractive index increases with energy in the transparent region to reach a maximum in the UV region at $\sim 3.0$ eV, and then declines to a minimum at 10.0 eV. The origin of the structures in the imaginary part of the dielectric function furthermore interprets the structure in the refractive index. The energy loss function $L(\omega)$, which describes the loss of energy when electrons pass through a uniform dielectric material, can be calculated from the dielectric constant as

$$L(\omega) = \mathrm{Im}\left(\frac{-1}{\varepsilon(\omega)}\right) = \frac{\varepsilon_2(\omega)}{\left[\varepsilon_1^2(\omega) - \varepsilon_2^2(\omega)\right]}. \qquad (3)$$

$L(\omega)$ is an important factor describing the energy loss for a very quick electron traversing through a material. The major peaks in $L(\omega)$ spectra represent the characteristics associated with plasma resonance, and the corresponding frequency is the so-called plasma frequency $\omega_P$ [28]. $L(\omega)$ peaks correspond to trailing edges in the reflection spectra; for example, the highest $L(\omega)$ peaks (Fig. 6c) are located at energy values corresponding to sudden decreases in $R(\omega)$. The reflectivity spectrum for MMTD in Fig. 6d reveals that the transition between bands occurs mainly in the energy range 2.0–14.0 eV. The average refractive index is up to 10%, showing that MMTD has very less metal reflective properties in this energy range. Most of the incident light is reflected when the refractive index is small. This indicates that N p and C p electrons are at a very deep level, in agreement with the band structure and the calculated DOS.

## 4. Conclusion

The electronic structure of MMTD was studied using the FP-LAPW method based on DFT with LDA, GGA, and mBJ as the exchange correlation functional. The electronic band structure shows a direct bandgap at the $\Gamma$ point of the BZ. The corresponding DOS were presented and the major structures were identified. The lower conduction band is a complex mixture of p states of S, C and N atoms. Analysis of the partial DOS revealed hybridization between N p, C p, N s, and H s orbitals. Using the projected DOS and band structure, we analyzed the interband contribution to the dispersion of optical parameters of MMTD. We also calculated the electronic charge density in the $(1\,1\,0)$ and

$(1\,0\,-1)$ planes, which revealed that the crystal has considerable anisotropy that favors enhanced optical susceptibility. We also calculated effective mass ratios for electrons, heavy holes, and light holes of 0.0577, 0.1126, and 0.0757, respectively. The real and imaginary parts of the dielectric function were also calculated, as well as the refractive index and extinction coefficient. The absorption edge is located at 2.9 eV. This edge arises from transition of N p states positioned at the VBM to C p states dominating the CBM.

## References

[1] G. Kornis, in: A.R. Katritzky, C.W. Rees (Eds.), Comprehensive Heterocyclic Chemistry, Pergamon Press, Oxford, 1984.
[2] E. Shouji, D.A. Buttry, J. Phys. Chem. B 102 (1998) 1444–1449.
[3] F. Hipler, S.G. Girol, R.A. Fischer, C. Wöll, Mater. Wiss. Werkstofftechn. 31 (2000) 872–877.
[4] A.R. Katritzky, Z. Wang, R.J. Offerman, J. Heterocyc. Chem. 27 (1990) 139–142.
[5] E.S. Raper, Coord. Chem. Rev. 153 (1996) 199–255;
E.S. Raper, Coord. Chem. Rev. 165 (1997) 475–567.
[6] P.A. Ortega, L.R. Vera, M. Campos-Vallette, G. Diaz Fleming, Spectrosc. Lett. 29 (1996) 477–496;
A.C. Fabretti, G.C. Franchini, G. Peyronel, M. Bellei, Spectrochim. Acta A 37 (1981) 587–590;
M.M. Osman, M.A. Makhyoun, A.B. Tadros, Bull. Soc. Chim. Fr. 11–12 (1980) I451;
S.A.A. Zaidi, M.R. Gajendragad, U. Agarwala, Z. Anorg. Allg. Chem. 415 (1975) 84–96;
M.R. Gajendragad, U. Agarwala, Aust. J. Chem. 28 (1975) 763–771.
[7] E.E. Lawson, H.G.M. Edwards, A.F. Johnson, Spectrochim. Acta A 53 (1997) 2571–2577;
H.G.M. Edwards, A.F. Johnson, E.E. Lawson, J. Mol. Struct. 351 (1995) 51–63;
E.E. Lawson, H.G.M. Edwards, A.F. Johnson, J. Raman Spectrosc. 26 (1995) 617–622.
[8] F. Hipler, M. Winter, R.A. Fischer, J. Mol. Struct. 658 (2003) 179–191.
[9] F. Hipler, R.A. Fischer, Muller, J. Chem. Soc. Perkin Trans. 2 (2002) 1620–1626.
[10] D. Koller, F. Tran, P. Blaha, Phys. Rev. B 83 (2011) 195134–195144.
[11] E. Engel, Phys. Rev. B 80 (2009) 161205.
[12] S. Jiang, T. Lu, Y. Long, J. Chen, J. Appl. Phys. 111 (2012) 043516.
[13] V.I. Anisimov, J. Zaanen, O.K. Andersen, Phys. Rev. B 44 (1991) 943–954.
[14] F. Tran, P. Blaha, Phys. Rev. Lett. 102 (2009) 226401.
[15] P. Blaha, K. Schwarz, J. Luitz, WIEN97, A full potential linearized augmented plane wave package for calculating crystal properties, Technical University, Vienna, 1991.
[16] A.D. Becke, E.R. Johnson, J. Chem. Phys. 124 (2006) 221101–221105.
[17] F. Tran, P. Blaha, K. Schwarz, J. Phys. Condens. Matter 19 (2007) 196208.
[18] I. Khan, A. Afaq, H.A.I. Ahmad, Comput. Mater. Sci. 61 (2012) 278–282.
[19] W. Khan, A.H. Reshak, Comput. Mater. Sci. 89 (2014) 52–56.
[20] A.H. Reshak, W. Khan, J. Alloys Cmpd. 592 (2014) 92–99.
[21] A.H. Reshak, S.A. Khan, J. Alloys Cmpd. 595 (2014) 125–130.
[22] A.H. Reshak, S.A. Khan, Mater. Res. Bull. 48 (2013) 4555–4564.
[23] B. Amin, R. Khenata, A. Bouhemadou, I. Ahmad, M. Maqbool, Physica B 407 (2012) 2588–2592.
[24] B. Amin, I. Ahmad, M. Maqbool, S. Goumri-Said, R. Ahmad, J. Appl. Phys. 109 (2011) 023109.
[25] M. Maqbool, B. Amin, I. Ahmad, J. Opt. Soc. Am. B 26 (11) (2009) 2181–2184.

[26] B. Amin, I. Ahmad, M. Maqbool, N. Ikram, Y. Saeed, A. Ahmad, S. Arif, J. Alloys Cmpd. 493 (2010) 212–218.

[27] S. Azam, J. Bila, H. Kamarudin, A.H. Reshak, Int. J. Electrochem. Sci. 9 (2014) 445–459.

[28] S. Azam, A.H. Reshak, Int. J. Electrochem. Sci. 8 (2013) 10359–10375.

[29] I.V. Kityk, A.S. Krochuk, J. Phys. Chem. Solids 53 (1992) 1315–1320.

[30] A.H. Reshak, J. Chyský, S. Azam, Int. J. Electrochem. Sci. 9 (2014) 460–477.